cancers

MDPI

Article

Discovery of VIP236, an αvβ3-Targeted Small-Molecule–Drug Conjugate with Neutrophil Elastase-Mediated Activation of 7-Ethyl Camptothecin Payload for Treatment of Solid Tumors

Hans-Georg Lerchen [1,*], Beatrix Stelte-Ludwig [1], Melanie Heroult [2], Dmitry Zubov [3], Kersten Matthias Gericke [3], Harvey Wong [4], Melanie M. Frigault [4], Amy J. Johnson [4], Raquel Izumi [4] and Ahmed Hamdy [4]

[1] Vincerx Pharma GmbH, 40789 Monheim, Germany; beatrix.stelte-ludwig@vincerx.com
[2] Bayer AG, 65926 Frankfurt, Germany; melanie.heroult@bayer.com
[3] Bayer AG, 42096 Wuppertal, Germany; dmitry.zubov@bayer.com (D.Z.); kerstenmatthias.gericke@bayer.com (K.M.G.)
[4] Vincerx Pharma, Inc., Palo Alto, CA 94306, USA; harvey.wong@vincerx.com (H.W.); melanie.frigault@vincerx.com (M.M.F.); amy.johnson@vincerx.com (A.J.J.); raquel.izumi@vincerx.com (R.I.); ahmed.hamdy@vincerx.com (A.H.)
* Correspondence: hans-georg.lerchen@vincerx.com

Simple Summary: The goal of this work was to improve the tumor selectivity of chemotherapy to reduce side effects and improve efficacy. We designed a drug called VIP236 that delivers chemotherapy directly to tumors due to a specialized "homing feature" that binds to αvβ3 integrins. Solid tumors express high levels of αvβ3 integrins. In contrast, expression of αvβ3 is low in healthy tissues. This difference in expression levels leads to preferential homing of the chemotherapy to tumor cells over healthy tissue to reduce side effects. In human cancer models conducted in mice, VIP236 was shown to substantially accumulate in tumors compared with normal tissue. The high accumulation of VIP236 in the tumors resulted in high and long-lasting tumor regression and reduced metastasis formation in brain and lung in cancer models.

Abstract: The emerging field of small-molecule–drug conjugates (SMDCs) using small-molecule biomarker-targeted compounds for tumor homing may provide new perspectives for targeted delivery. Here, for the first time, we disclose the structure and the synthesis of VIP236, an SMDC designed for the treatment of metastatic solid tumors by targeting αvβ3 integrins and extracellular cleavage of the 7-ethyl camptothecin payload by neutrophil elastase in the tumor microenvironment. Imaging studies in the Lewis lung mouse model using an elastase cleavable quenched substrate showed pronounced elastase activity in the tumor. Pharmacokinetics studies of VIP236 in tumor-bearing mice demonstrated high stability of the SMDC in plasma and high tumor accumulation of the cleaved payload. Studies in bile-duct-cannulated rats showed that biliary excretion of the unmodified conjugate is the primary route of elimination. Treatment- and time-dependent phosphorylation of H2AX, a marker of DNA damage downstream of topoisomerase 1 inhibition, verified the on-target activity of the payload cleaved from VIP236 in vivo. Treatment with VIP236 resulted in long-lasting tumor regression in subcutaneous patient-derived xenograft (PDX) models from patients with non-small-cell lung, colon, and renal cancer as well as in two orthotopic metastatic triple-negative breast cancer PDX models. In these models, a significant reduction of brain and lung metastases also was observed.

check for updates

Citation: Lerchen, H.-G.; Stelte-Ludwig, B.; Heroult, M.; Zubov, D.; Gericke, K.M.; Wong, H.; Frigault, M.M.; Johnson, A.J.; Izumi, R.; Hamdy, A. Discovery of VIP236, an αvβ3-Targeted Small-Molecule–Drug Conjugate with Neutrophil Elastase-Mediated Activation of 7-Ethyl Camptothecin Payload for Treatment of Solid Tumors. *Cancers* **2023**, *15*, 4381. https://doi.org/10.3390/cancers15174381

Academic Editor: Alexander Shtil

Received: 30 June 2023
Revised: 21 August 2023
Accepted: 22 August 2023
Published: 1 September 2023

1. Introduction

Following Paul Ehrlich's vision of a magic bullet ("Zauberkugel"), intense research efforts are ongoing to improve the therapeutic index of antineoplastic agents or radionuclides by restricting their systemic delivery to tumor tissue [1]. With the approval of 13 antibody drug conjugates (ADCs), these are now among the fastest growing drug class in oncology [2–5]. The ADC mode of action is well understood and follows the route of

target binding mediated by the antibody and subsequent internalization and trafficking of the ADC to the lysosomes where the active metabolite is released. The expansion of payload classes beyond tubulin binders by employing topoisomerase I (TOP1) inhibitors as payloads in ADCs such as trastuzumab deruxtecan (Enhertu®) [6] and sacituzumab govitecan (Trodelvy®) [7] was one of the drivers of recent successes. However, clinical use of ADCs is limited by substantial toxicity in patients, and dose-limiting toxicities are often shared across the same cytotoxic payload regardless of the antibody target. Clinical evidence suggests that the tolerated doses of ADCs are not significantly different from those of related small molecules [8].

The emerging field of small-molecule–drug conjugates (SMDCs) for targeted delivery is less established but has the potential to overcome some of the ADC-related issues. Due to a significantly reduced molecular size, SMDCs are non-immunogenic and may have an improved penetration into tumor tissue. Furthermore, synthetic accessibility is less complex and less expensive [9,10]. Examples of targets explored for SMDC delivery with small molecule or peptide ligands include the folate receptor [11], αvβ3 integrin [12–16], carbonic anhydrase IX [17], somatostatin receptor 2 [18], fibroblast activation protein [19], ephrin A2 [20], sortilin [21], and nectin 4 [22]. Looking for targets that are broadly expressed in solid tumors and associated with aggressive disease, we were particularly interested in αvβ3 integrins. αvβ3 Integrins are heterodimeric transmembrane receptors that are overexpressed on activated endothelial cells [23] and on several tumor cell types including metastatic tumors [24]. These receptors bind to arginine–glycine–aspartate (RGD)-containing matrix proteins and have an important function in tumor-induced angiogenesis. In the tumor microenvironment (TME), αvβ3 integrins play critical roles in tumor progression, resistance to cytotoxic therapy, metastasis, and the recruitment of immune and inflammatory cells [25]. Expression of αvβ3 integrin is associated with poor prognosis in melanoma [26], cell invasion in hepatocellular carcinoma [27], and metastasis of chondrosarcoma [28].

Neutrophil elastase (NE) belongs to the serine family of proteases and degrades elastin and other extracellular matrix proteins, which contribute to cancer progression by enhancing tumor evasion and metastasis [29]. It is expressed by neutrophils, macrophages, and tumor stroma and is found elevated in lung, breast, and kidney tumors but remains low in normal tissues [30]. Elastase expression and neutrophil tumor infiltration have been correlated with metastatic potential and poor prognosis. Survival of patients with breast cancer and non-small-cell lung cancer (NSCLC) is poor in those individuals expressing high NE as compared with those expressing low NE levels [31]. ADCs with NE-sensitive linkers are currently being explored [32,33].

We recently described a novel SMDC designed for αvβ3-targeted delivery of an optimized camptothecin payload to cancer cells with NE-mediated payload release, as illustrated in Figure 1A [34]. Efficient tumor homing of the peptidomimetic integrin binder employed in the SMDC was demonstrated in imaging studies. Furthermore, we showed in vitro data of the optimized camptothecin payload supporting the potential to overcome transporter substrate liabilities associated with resistance to SN38, the active metabolite of irinotecan. The favorable PK profile resulted in a robust anticancer activity in cell-line-derived models representing different tumor indications [34].

Herein, for the first time, we disclose the synthesis and structure of the SMDC VIP236 consisting of the three modules outlined in Figure 1B and further elucidate VIP236 pharmacokinetics, pharmacodynamics, and activity in patient-derived xenograft models including metastatic models.

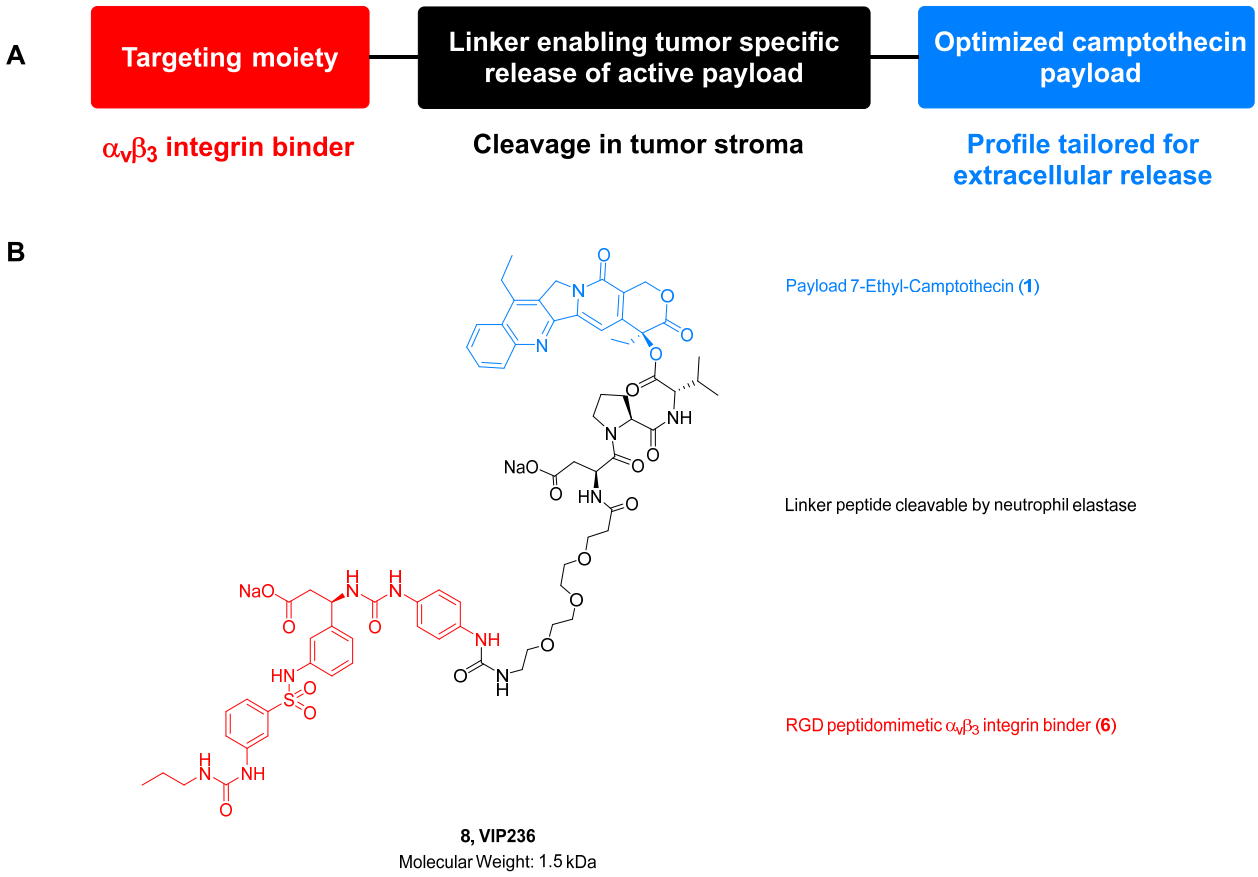

Figure 1. (**A**) Design of a targeted small-molecule–drug conjugate (SMDC) with a tailored match of the individual modules for treatment of aggressive cancers. (**B**) Structure of VIP236 with molecular weight of ~1.5 kDa.

2. Material and Methods

2.1. Imaging Study Showing Elastase-Activity in Tumors

To confirm the presence of free active NE in tumors, an elastase substrate peptide labelled by infrared fluorophore and corresponding quencher (Lys(QSY21)-ANPV-Cys(AlexaFluor647)) was ordered for custom synthesis at Anaspec, Fremont, CA, USA. Cleavage of the substrate by NE leads to a strong increase in AlexaFluor647 fluorescence at 680 nm after excitation at 625 nm. Then, 200 nmol of the quenched peptide dissolved in 100 µL phosphate-buffered saline (PBS) was injected into the tail vein of anesthetized mice carrying a Lewis lung tumor of around 1500 mm^3 volume. Mice were imaged in the infrared imager (Kodak In Vivo Multispectral Imaging System FX, Kodak, Rochester, NY, USA) 10 and 90 min after injection.

2.2. Compounds

The SMDC VIP236 (**8**) and its epimers **8e1** and **8e2** were synthesized in the Medicinal Chemistry Research Labs of Bayer AG, Pharmaceuticals, Wuppertal, as outlined in the Results Section 3.2, with further details and analytical data provided in the Supplementary Information.

2.3. Stability in Rat Plasma and in Buffer at pH 7.4

The SMDC VIP236 was dissolved in acetonitrile/DMSO (1:1, 0.5 mL). While vortexing, 20 µL of this solution was added to 1 mL 37 °C rat plasma. The incubation was stopped at respective time intervals by adding acetonitrile/buffer pH3 (80:20) and VIP236, and formation of degradation products was analyzed by LC and LC/MS.

For hydrolytic stability measurement, VIP236 was dissolved in PBS buffer at pH 7.4 in a concentration of 5 mg/mL, and the solution was stored at 4 °C. LC/MS were measured after 2, 6, 30, and 79 days.

2.4. Metabolic Stability in Hepatocytes

VIP236 (1 µM) was incubated separately in duplicate in a 24-well plate containing mouse, rat, dog, or human hepatocyte suspensions (1 million cells/mL) at 37 °C for 4 h under 5% CO_2:95% air. Aliquots (50 µL) were taken at 0, 15, 30, 60, 120, 180, and 240 min, and the samples were treated with acetonitrile (200 µL) containing an internal standard (100 ng/mL tolbutamide). The samples were centrifuged (4000 rpm for 10 min), and aliquots (100 µL) of the supernatant were taken and mixed with water (100 µL). A 5 µL aliquot was analyzed by LC/MS/MS for loss of VIP236.

2.5. Human and Mouse NE Biochemical Cleavage Assay

Different volumes of VIP236 were added to microtiter plate wells to final concentrations ranging from 0–50 µM. Then, 125 µL of pre-heated buffer (100 mM Tris pH 7.5, 150 mM NaCl, 10 mM $CaCl_2$, and 0.05% BSA) was added to each incubation. The reaction was started by adding 0.5 or 1 nM activated mouse elastase (according to manufacturer's protocol) or human NE to the reaction vials. A negative control without elastase was run under the same conditions. The reaction was stopped at 0, 4.5, 8, and 12 min by the addition of acidified acetonitrile/0.2% formic acid. Camptothecin was used as internal standard for the LC/MS/MS analysis. The kinetic parameters describing the cleavage of VIP236 by NE were estimated by fitting to the Michaelis–Menten equation.

2.6. In Vitro Proliferation Assay in the Presence and Absence of NE

The in vitro cytotoxicity was evaluated in cancer cell lines NCI-H292 and LoVo after a 72-h continuous exposure to the presence or absence of 20 nM NE using MTT assays (ATCC, Manassas, VA, USA). IC_{50} values were determined as the concentration of compound required for 50% inhibition of cell viability.

2.7. In Vivo Pharmacokinetics in Tumor-Bearing Mice

Female NMRI nu/nu mice bearing 786-O tumors were given a 4 mg/kg VIP236, **8e1** (VIP407), or **8e2** (VIP940) dose or an equimolar 1 mg/kg dose of **1** intravenously (IV) via tail vein. Following delivery of VIP236, the control epimers **8e1** or **8e2**, or unconjugated payload **1**, tumor-bearing mice (n = 2 per timepoint) were sacrificed at pre-dose, 0.033, 0.167, 0.5, 1, 2, 4, 7, and 24 h post dose. Plasma and tumor samples were collected and frozen at <−15 °C until sample analysis. Samples were analyzed for concentrations of respective SMDCs and the released payload **1** by LC/MS/MS. Pharmacokinetics of VIP236 [34] in comparison to **8e1**, **8e2**, and payload **1** [34] were determined using geometric mean concentration–time profiles. All pharmacokinetic parameters were calculated by non-compartmental methods [35].

2.8. VIP236 Bile-Duct-Cannulated Rat Study

Male bile-duct-cannulated rats (n = 3) were administered a 10 mg/kg intravenous bolus dose of VIP236 via a jugular vein catheter. Bile was collected from 0–4, 4–8, 8–24, and 24–48 h after dosing; urine was collected from 0–8, 8–24, and 24–48 h after dosing; and feces were collected from 0–24 and 24–48 h after dosing. LC/MS/MS was used to quantify VIP236 and payload **1** in samples of bile and urine. Feces were not analyzed, as there was complete recovery of the entire VIP236 dose in bile and urine.

2.9. IHC Analysis

At least 50 patient-derived samples for each reported indication were evaluated for specific αvβ3 staining using anti-αvβ3 antibody (monoclonal/Rabbit/Clone EM22703, Sigma; 1:50 dilution, incubation time 32 min at room temperature [RT]). For staining,

the Detection kit Ultra View Universal DAB (Ventana, Oro Valley, AZ, USA) was used (incubation time 8/8/4 min incubation at 37 °C). For evaluating the presence of human NE, the tissue samples were evaluated using anti-NE antibody (Abcam (Boston, MA, USA)/ab68672; 1:150 dilution, incubation time 20 min at RT). For staining, the Bond Polymer Refine Detection kit (Leica (Wetzlar, Germany)/Menarini (Florence, Italy)) was used (incubation time 8/8/10 min at RT). All samples were evaluated by a pathologist.

The tissues of 5 animals per group were examined according to standard protocol and in parallel evaluated for necrotic areas and connective tissue. The analysis was restricted to viable neoplastic cells. The semiquantitative IHC-scoring scale (0 to 3) was related to percent staining of neoplastic cell (0: no stain; 1: up to 25% of the cells show positive immunoreactivity; 2: 25–50% of the cells show positive immunoreactivity; 3: 50–100% of cells show positive immunoreactivity) to deduce a composite score. Light microscopic images acquired at 200× magnification and evaluation of 10 high-power fields were averaged for each sample. Antibodies used: TOP1 antibody (Abcam Ab109374, dilution 1:100 in PBS), incubation 60 min at room temperature (RT); αvβ3 antibody (Bioss bs-1310R, Woburn, MA, USA, dilution 1:200 in PBS) incubation time 60 min at RT; NE antibody (Booster Bio PB10058, Pleasanton, CA, USA, dilution 1:100 in PBS: incubation time overnight at 4 °C). A positive and negative tissue control for the respective marker was included in the staining process. Counterstain was performed with Mayer's hematoxylin with a 1 min staining time at RT.

2.10. H2AX Staining as a Marker for DNA Damage in SNU16 CDX Mouse Model

A total of 72 xenograft tumor samples were analyzed for their content of γH2AX by means of a validated IHC assay (Nuvisan, Neu-Ulm, Germany). All samples were fixed in 10% neutral buffered formalin immediately after tumor excision and subsequently stored in 70% ethanol at 4 °C and processed into paraffin after 24 h of fixation. Mouse anti-γH2AX (Merck Ab#05-636, Darmstadt, Germany) was used with Envision System and DAB+ Chromogen/Substrate Buffer (Dako/Agilent, Santa Clara, CA, USA) for analysis of γH2AX IHC. A ScanII slide scanner was used to digitize IHC images for quantification (QuPath; https://qupath.github.io (accessed on 20 August 2023)) of the percentage of γH2AX-positive cells and represented in a histogram with standard deviation.

2.11. PDX Models

Studies were conducted according to all applicable international, national, and local laws and followed the national guidelines for the Care and Use of Laboratory Animals of the Society of Laboratory Animal Science (GV-SOLAS). All animal experiment protocols were approved by the Regional Council Committee on the Ethics of Animal Experiments. Non-small-cell lung (LXFL529) and renal (RXF2667) PDX mouse models comprised six groups each with 10 animals. Tumor fragments (3–4 mm edge length) were transplanted, and tumor growth was monitored until a median size of about 120–150 mm^3 was achieved. VIP236 was administered intravenously in a 3 days on/4 days off (vehicle, 20 and 40 mg/kg) or 2 days on/5 days off (30 and 40 mg/kg) dosing schedule as well as once weekly (60 mg/kg). Both experiments were terminated after a three-week recovery phase on day 63. Animals were monitored at least twice daily on working days and at least once daily on weekends (tumor size and body weight measurement). Colon (CXF2068) and triple-negative breast cancer (TNBC) (MAXF BR120) PDX mouse models were performed as described above with changes in schedule. VIP236 was administered in a 2 days on/5 days off (vehicle, 20 mg/kg and 40 mg/kg), once weekly (60 mg/kg), or 2 days on/12 days off (40 mg/kg) schedule. The statistical significance of antitumor efficacy was analyzed by the non-parametric Kruskal–Wallis test, followed by Dunn's method for multiple comparisons using GraphPad Prism bioanalytic software (version 9.10), with $p < 0.05$ as significant. Additionally, a nonpaired *t*-test was performed using GraphPad Prism (version 9.10).

2.12. Orthotopic TNBC Model MA4296 and MA15191

Two orthotopic TNBC PDX mouse models were performed. Tumor cells were inoculated into the mammary fat pad of mice. Therefore, the mice were anesthetized shortly before surgery. After disinfection of the skin, mice received a small incision in the skin between the 4th and 5th dug. Each mouse was implanted with 2.5×10^6 (MA4296) or 5×10^6 (MA15191) cells. Treatment started on day 20 after inoculation, when palpable tumor sizes reached 127 mm^3 (day 33 for MA15191). VIP236 was administered via intravenous injection with 40 mg/kg of VIP236 at two successive days followed by 5 days off or with 60 mg/kg of VIP236 once weekly for 4 weeks. Tumors were measured twice weekly with calipers, and their volume was calculated with the following formula: (length $\times$ width^2)/2. The body weight was also determined two times weekly. Reasons for termination were tumor size > 1.5 cm^3 or poor general condition. At the end of the study, tissue sampling for IHC and PCR analyses was performed. The statistical analysis was performed using mixed-effect analysis with Tukey's multiple comparisons test (GraphPad Prism 8.4.2) to calculate significance in tumor growth inhibition between vehicle and treatment groups over time. The Kruskal–Wallis test was used to determine significance at study days 43 and 47. Additionally, the unpaired *t*-test was performed.

2.13. PCR Analysis

To detect human tumor cells, a human-specific RealTime DNA PCR using an optimized primer-probe-assay targeting the alpha-satellite region of the human chromosome 17—a locus, which is sufficiently different from similar loci in the mouse genome—was performed [36]. Genomic DNA was isolated from liver, lung, and brain of all mice per group using the Qiagen Dneasy Blood & Tissue Kit (Qiagen GmbH, Hilden, Germany) as recommended by the manufacturer.

For RealTime PCR, the ready-to-use primer-probe-assay and the TaqMan® Universal PCR Master Mix, No AmpErase® UNG (Applied Biosystems GmbH, Weiterstadt, Germany, Prod-No. 4324018) were used. The PCR reaction and quantification were performed in a StepOnePlus™ RealTime PCR System (LightCycler 480 II system (Hoffmann-La Roche, Basel, Switzerland) applying the standard protocol supplied by the manufacturer. For semi-quantitative evaluation, the crossing point (Cp) value, also known as cycle threshold, was used. Cp values correlate inversely with the DNA load, with values ≥ 35 considered negative. Genomic DNA from an appropriate human tumor xenograft as a positive control, from NOD/SCID mouse liver as a negative control, as well as a water sample as a reagent control were processed in parallel. The statistical analysis was performed using GraphPad Prism version 8.4.2 for Windows, GraphPad Software, La Jolla, CA, USA.

3. Results

3.1. Tumor-Associated NE Cleavage

The presence of free and active NE in tumors was evaluated in the Lewis lung carcinoma tumor model by IV injection of the fluorescently labelled elastase-specific substrate. The elastase recognition sequence (NPV) in this quenched substrate was very similar to elastase sensitive peptide linker DPV, which was employed in VIP236 with comparable elastase cleavage efficacy and selectivity. Substrate cleavage corresponding to the increase in the fluorescent signal was monitored in the infrared fluorescent imager at excitation wavelength of 625 nm and emission wavelength of 680 nm. Strong fluorescent signal was observed in tumor tissue 10 and 90 min after injection, and lower/no detectible substrate cleavage in other tissues and organs indicated increased NE enzymatic activity in the tumor tissue. Superposition of X-ray and fluorescent images are depicted in Figure 2.

3.2. Synthesis of VIP236 and Epimers

The small-molecule–drug conjugate VIP236 was designed to target $\alpha v\beta 3$ integrins in tumor tissue and to release the payload 7-ethyl camptothecin **1** [37,38] upon enzymatic cleavage by NE in a traceless manner. The RGD-peptidomimetic $\alpha v\beta 3$ ligand **6** has shown

efficient tumor homing when coupled to a fluorescent dye [34]. In the SMDC VIP236, this integrin ligand **6** is now attached via a short PEG-spacer to a tripeptide L-aspartic acid-L-proline-L-valine, which at the C-terminal end is linked through an ester bond to the hydroxy-lactone ring of the 7-ethyl-camptothecin payload **1** [37,38]. The 7-ethyl camptothecin payload **1** was selected to meet the physicochemical and permeability properties tailored for extracellular release in the TME and to address liabilities of SN38, the active metabolite of irinotecan and sacituzumab govitecan [7,39]. The linker peptide was selected to be a substrate sequence of NE and at the same time to provide maximal stability of the ester bond connecting the payload due to steric hindrance. The synthesis of VIP236, consisting of three modules, namely the peptidomimetic αvβ3 binder **6**, the NE cleavable linker, and the 7-ethyl camptothecin payload **1**, is outlined in Scheme 1. As additional tool compounds suitable to investigate the contribution of the individual modules of VIP236 to the payload delivery to tumor cells, the two most relevant epimers **8e1** and **8e2** were synthesized following the same route (Scheme 1).

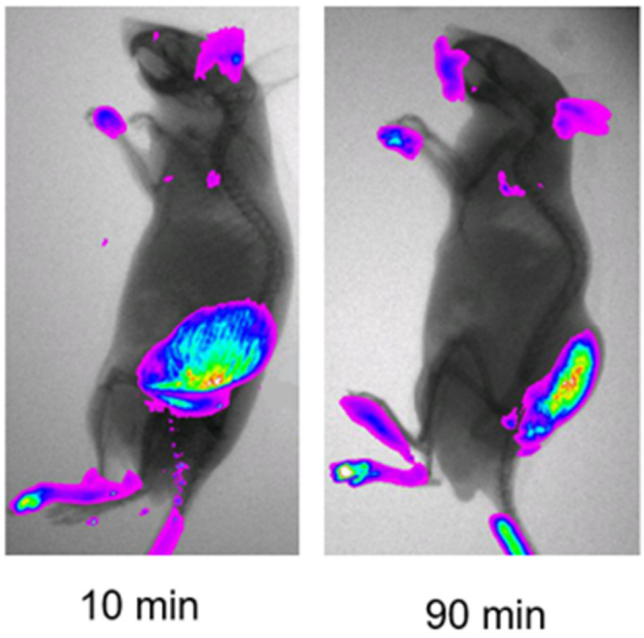

Figure 2. Infrared fluorescent imaging of the Lewis lung tumor-bearing mice after injection of 200 nmol of the elastase sensitive quenched substrate. Strong fluorescence is observed in tumor 10 and 90 min post injection, indicating increase in active elastase enzyme in the tumor tissue and no/lower activity in other organs.

For an efficient NE-mediated release of the active payload **1** from the SMDC VIP236, the ester bond between L-valine and payload **1** needs to be cleaved at the C-terminal end of the linker peptide aspartic acid-proline-valine, which was found to be a substrate tripeptide of NE. Replacement of L-valine in the SMDC VIP236 by the unnatural amino acid D-valine provided the epimer **8e1**, deemed to be a non-cleavable SMDC, which served as a control to show the impact of elastase cleavage for activity.

In the control SMDC **8e2**, the peptidomimetic integrin ligand **6e2** with S-configuration at the stereocenter instead of R-configuration in **6** was employed, which has a major impact on the affinity to αvβ3 integrins. **8e2** represents a weakly binding epimer with ~25-fold reduced binding affinity to αvβ3 integrins as compared with VIP236 [40]. Therefore, **8e2** is an appropriate control to investigate the contribution of the integrin-binding moiety **6** to the tumor homing of the SMDC VIP236.

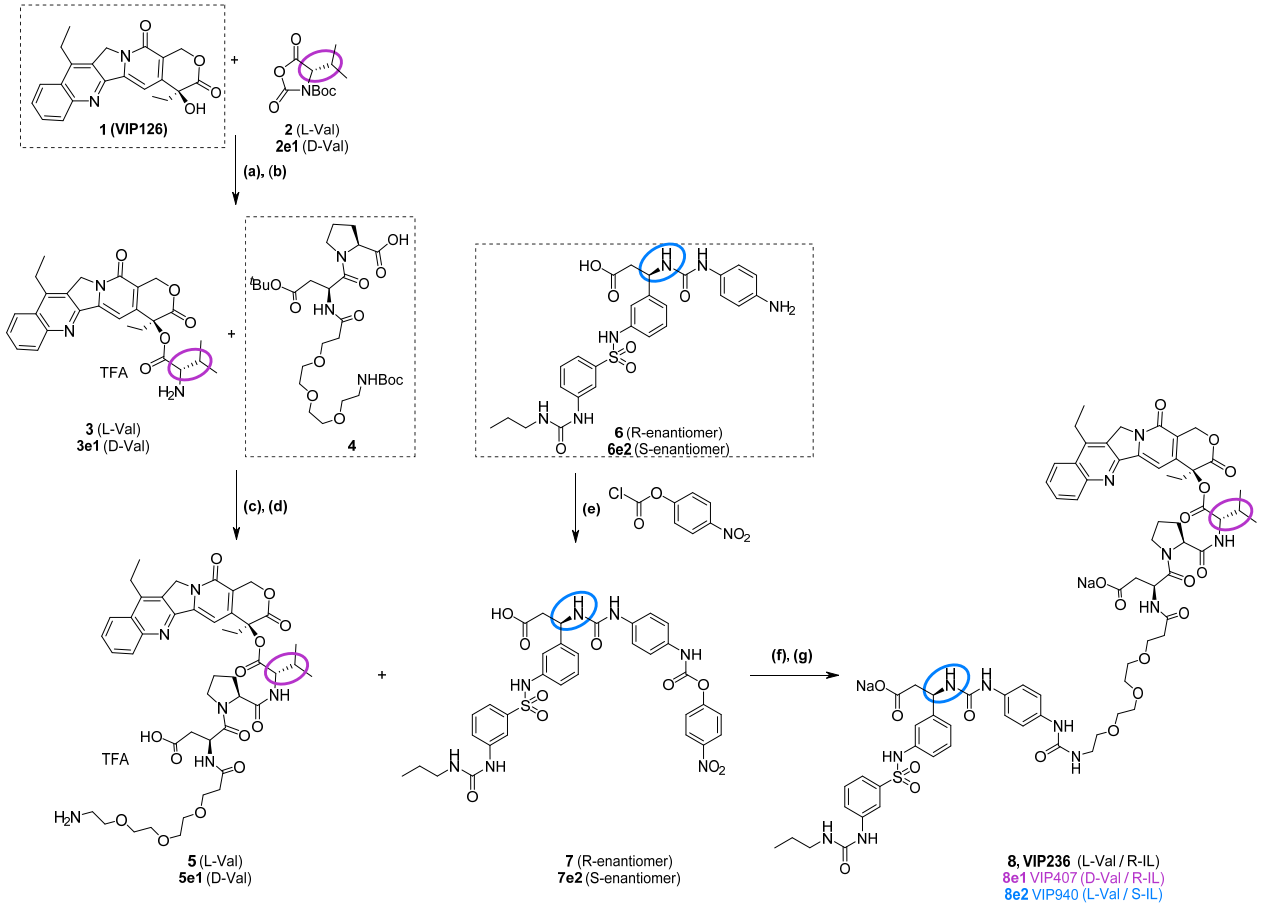

Scheme 1. Synthesis of the SMDC **8** (VIP236) and its epimers **8e1** (non-cleavable) and **8e2** (weakly binding).

The attachment of a valine residue to the 20-hydroxy group of 7-ethyl camptothecin is challenging due to steric hindrance and the risk of epimerization; it was accomplished as outlined in Scheme 1 by coupling of the activated building block Boc-valine-N-carboxy anhydride **2** in dichloromethane in the presence of DMAP (a). Subsequent deprotection (b) and acylation with the partially protected linker peptide **4** in the presence of EDCI, Oxyma, and diisopropylethylamine in DMF (c), followed by removal of the protecting groups with TFA in dichloromethane (d), provided the intermediate **5**. Coupling of **5** with the activated integrin ligand **7** in the presence of diisopropylethylamine in DMF (f) and subsequent transformation in acetone/water to the bis-sodium salt (g) provided the SMDC VIP236. Details of the synthesis outlined in Scheme 1 and analytical characterization are provided in the Supplementary Information. The epimers **8e1** and **8e2** were synthesized in analogy, starting with the enantiomers **2e1** instead of **2** and **6e2** instead of **6**, respectively. Enantiomeric purity of **7** and **7e2** is given in Table S1.

3.3. In Vitro Evaluation: VIP236 Is Highly Stable but Efficiently Cleaved by Mouse and Human NE

For efficient delivery of 7-ethyl camptothecin payload **1** to tumor tissue, high stability of the SMDC in circulation and as well as efficient cleavage by NE is critical. VIP236 is highly stable when dissolved in PBS buffer at a concentration of 5 mg/mL, with no degradation observed after 79 days of storage in solution at 4 °C (LC/MS measured after 79 days is shown in Figure S1). Furthermore, upon incubation in rat plasma at 37 °C, VIP236 was stable for over 24 h (Figure S2). VIP236 was also found to be very stable (>80% of parent drug remaining) in mouse, rat, dog, and human hepatocytes after a 4-h incubation.

The kinetic parameters describing the cleavage of SMDC VIP236 to payload **1,** i.e., the Michaelis–Menten constant (Km) and maximum turnover number (kcat) by human and

murine NE, were determined at enzyme concentrations of 0.5 and 1.0 nmol. The kinetic parameters estimated for the two enzyme concentrations were determined for the following:

Human NE (Figure S3):

- Km = 9.4 and 9.6 µM, respectively;
- kcat = 593 and 691 1/min, respectively.
- Mouse elastase (Figure S4):
- Km = 15.9 and 8.9 µM, respectively;
- kcat = 94 and 80 1/min, respectively.

Overall, Km of NE was similar when comparing the mouse and human enzyme.

To evaluate the requirement for NE to cleave the active payload, we evaluated the in vitro cytotoxic activity of VIP236 and respective epimers **8e1** and **8e2** in comparison to the payload **1** itself in NCI-H292 and LoVo cancer cell lines in the presence or absence of NE. Without NE, all SMDCs showed weak cytotoxic activity with IC_{50} values in the three-digit nanomolar range. Only when NE was added to the culture medium the cytotoxic activity of VIP236 and its weakly binding epimer **8e2** increased by about 25–100-fold to reach similar potency as the payload **1** alone in contrast to the non-cleavable epimer **8e1** (Table 1 and Figure S5).

Table 1. Cytotoxic activity (IC_{50}) of SMDCs in comparison to payload **1** in the presence or absence of 20 nM hNE in NCI-H292 and LoVo cancer cell lines. hNE, human neutrophil elastase.

SMDC	NCI H292 IC_{50} (nM)	NCI H292 + hNE IC_{50} (nM)	LoVo IC_{50} (nM)	LoVo + hNE IC_{50} (nM)
VIP236	209	1.78	98	3.0
8e1	5000	317	5520	412
8e2	127	1.54	68	3.2
1	1.54	1.35	1.9	1.85

3.4. In Vivo Pharmacokinetics and Bile Duct Cannulated Rat Study

VIP236, **8e1**, **8e2**, and payload **1** plasma and tumor concentration–time profiles after intravenous administration are presented in Figure 3. Pharmacokinetics parameters for the SMDCs are shown in Table S2. Clearance (CL) was low for all three SMDCs in tumor-bearing mice, with VIP236 CL < **8e2** CL < **8e1** CL. The volume of distribution at steady state (V_{ss}) was low for all three SMDCs and approximated plasma volume for VIP236 and **8e2** [41]. For **8e1**, V_{ss} was slightly larger, as it was approximately two times the plasma volume. Half-life was short for all compounds (~1 h).

After a single IV administration of VIP236, **8e2**, and **8e1** at 4 mg/kg, concentrations of the parent SMDCs were higher in plasma compared with tumor (Figure 3A,C,E). Delivery of payload **1** to the tumor was dependent on which SMDC was administered. When delivered via VIP236, the AUC_{tumor}/AUC_{plasma} ratio of released payload **1** was 6.1, which is ~11-fold higher compared to the AUC_{tumor}/AUC_{plasma} ratio of 0.61 measured after direct IV administration of payload **1** [34] and suggests that delivery of payload **1** via VIP236 concentrates the payload **1** in tumor tissue (Table 2). The weakly binding epimer **8e2** did not appear to preferentially deliver payload **1** to tumor tissue, while payload **1** was not detected in tumors after administration of the non-cleavable epimer **8e1**.

The recovery of the VIP236 dose in male bile-duct-cannulated rats is shown in Table 3. In non-tumor-bearing rats, almost the entire dose was recovered as unchanged VIP236 in bile (~100%) (Table 3). Small quantities of the VIP236 dose were recovered as unchanged VIP236 in urine (~2.4%). Only trace levels of cleaved payload **1** were quantified in bile and urine (<1% total;). Overall, the main route of elimination of VIP236 in rats appears to be via biliary excretion of unchanged VIP236.

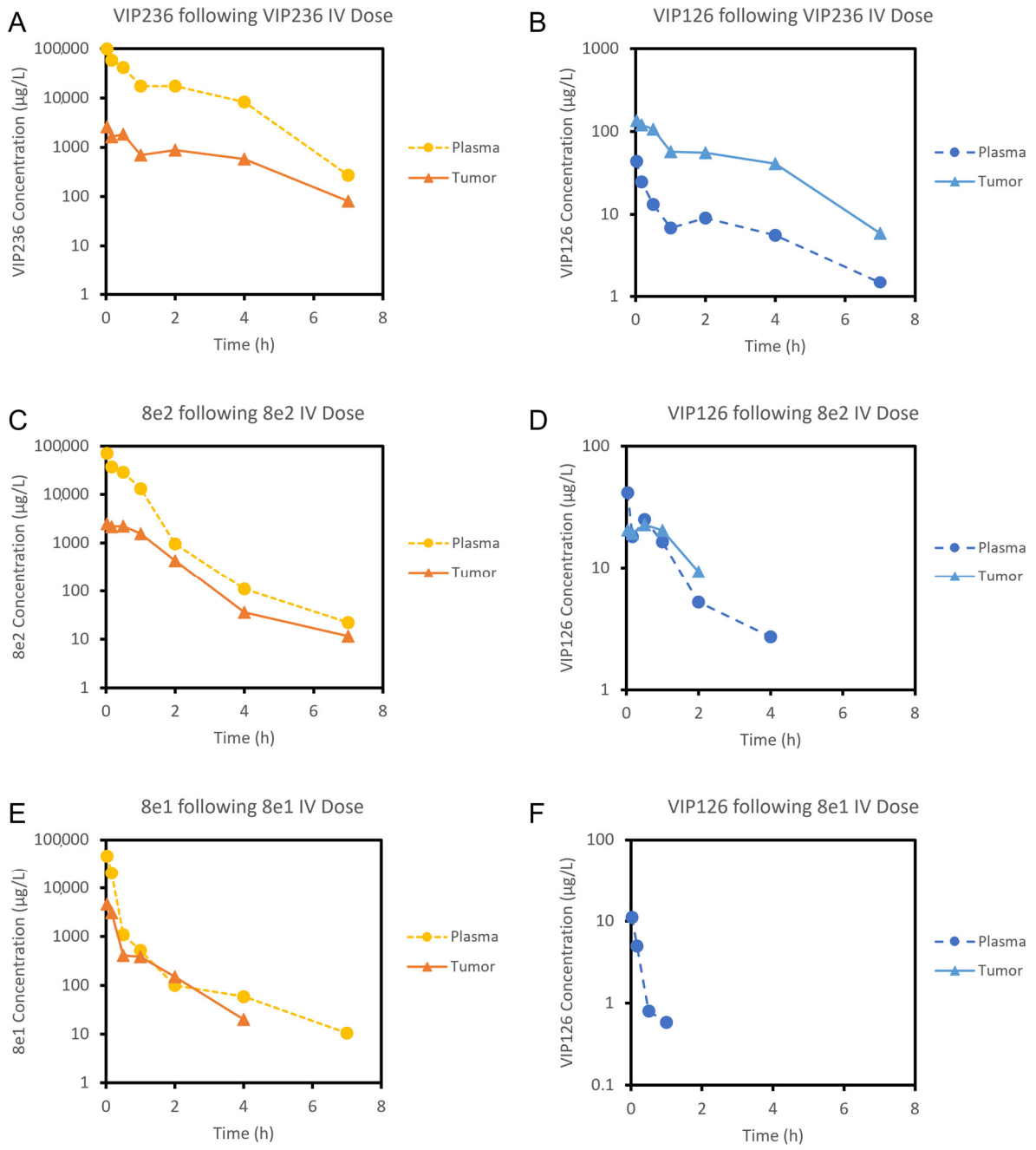

Figure 3. Geometric Mean Plasma and Tumor Concentration–Time Profiles for Parent Compound VIP236 (**A**) and Payload **1** (VIP126) (**B**) Following a 4 mg/kg Intravenous Dose of VIP236 to Female NMRI nu/nu Tumor-Bearing Mice. The corresponding plots are shown when the weakly binding epimer **8e2** (**C**,**D**) and the non-cleavable epimer **8e1** (**E**,**F**) are administered intravenously at a 4 mg/kg dose. Levels of payload **1** (VIP126) in tumor were below the assay LLOQ when **8e1** was dosed (**F**).

3.5. IHC Staining Confirms αvβ3 and NE Presence in Patient Tumor Samples

Patient tumor samples (≥50) from different cancer indications were evaluated to confirm αvβ3 and NE presence in advanced cancers where clinical data indicate correlation of NE expression and poor prognosis [31]. Poor survival also correlates with αvβ3 expression [42,43]. NE staining as well as αvβ3 staining on endothelial cells was detected, as shown in Figure 4. In some indications, additional membranous staining of αvβ3 on tumor cells was observed (e.g., renal cancer).

Table 2. Tumor/Plasma pharmacokinetics of payload **1** (VIP126) after intravenous administration of VIP236, **8e1** (non-cleavable epimer), **8e2** (weakly binding epimer), and payload **1** (VIP126) in 786-O tumor-bearing mice. LLOQ, less than the lower limit of quantitation.

Compound Dosed	VIP236 4 mg/kg IV	8e2 4 mg/kg IV	8e1 4 mg/kg IV	Payload 1 (VIP126) 1 mg/kg IV
Compound measured	VIP126	VIP126	VIP126	VIP126
AUC_{tumor} [μg·h/L]	318	50.4	<LLOQ	185
AUC_{plasma} [μg·h/L]	52.1	43.3	2.47	301
AUC_{tumor}/AUC_{plasma}	6.1	1.17	<LLOQ	0.616

Table 3. Percent of administered intravenous dose recovered as unchanged VIP236 in bile and urine in male BDC rats. * Recovery is the average of rat 1–3 and is within experimental error of ~100%.

Matrix	Animal	% of Dose Recovered in 48-h	Mean Recovery %
Bile	Rat 1	89.7	108 ± 17.2 *
	Rat 2	109	
	Rat 3	124	
Urine	Rat 1	2.8	2.4 ± 0.29
	Rat 2	2.3	
	Rat 3	2.3	

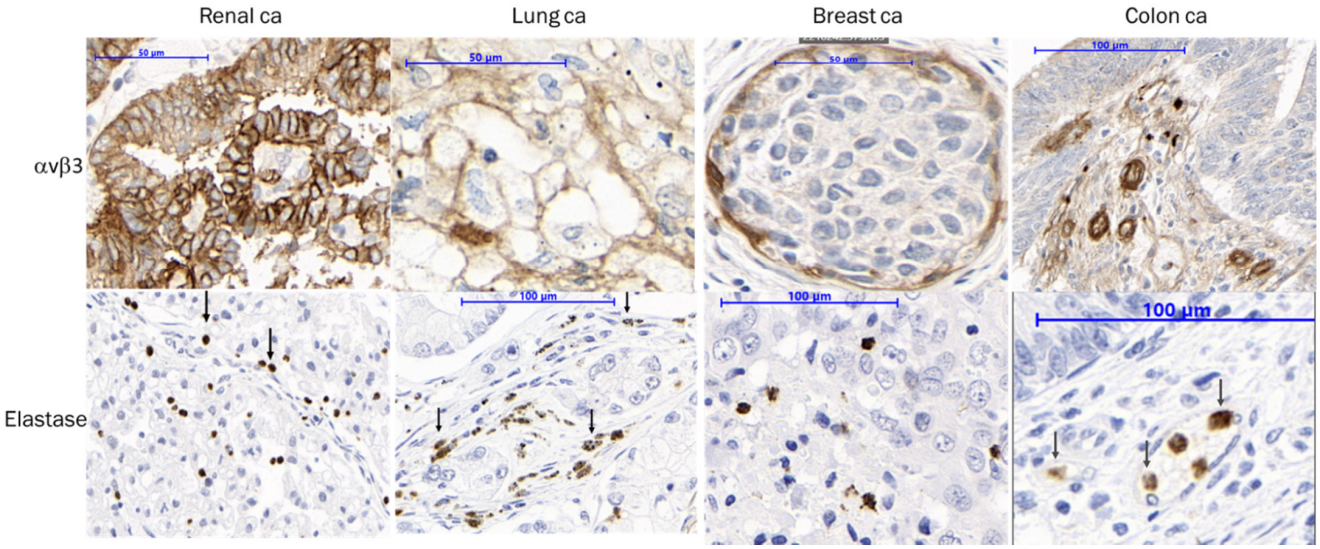

Figure 4. Representative images of IHC analysis of αvβ3 integrin and neutrophil elastase performed with patient samples for each indication shown (arrows): clear-cell renal carcinoma, non-small-cell lung cancer, triple-negative breast cancer, and microsatellite instability-negative colorectal carcinoma.

3.6. Time- and Dose-Dependent Induction of DNA Damage by VIP236

TOP1 inhibitors deliver DNA damage, which can be measured by phosphorylated H2AX (γH2AX) [44]. Therefore, the pharmacodynamic effect of the payload **1** of VIP236 was evaluated in an SNU16 (gastric cancer cell line) xenograft mouse model. As a certain amount of baseline DNA damage is expected, the pretreatment samples had 36% γH2AX-positive cells. A time-dependent increase in the percentage of γH2AX-positive cells was detected by IHC after treatment on day 2 (Figure 5A). At the 20 mg/kg dose level, robust induction of γH2AX was observed with a range of 68% to 79% γH2AX-positive cells between the 24.25–48 h timepoints (Figure 5B). The increase in γH2AX returned to baseline

levels 144 h after treatment. For some of the groups (e.g., the 144 h time point of the 20 mg/kg dose group), not enough tumor volume was available for preparation of samples for γH2AX IHC analysis since tumor volume had greatly decreased after one week of treatment.

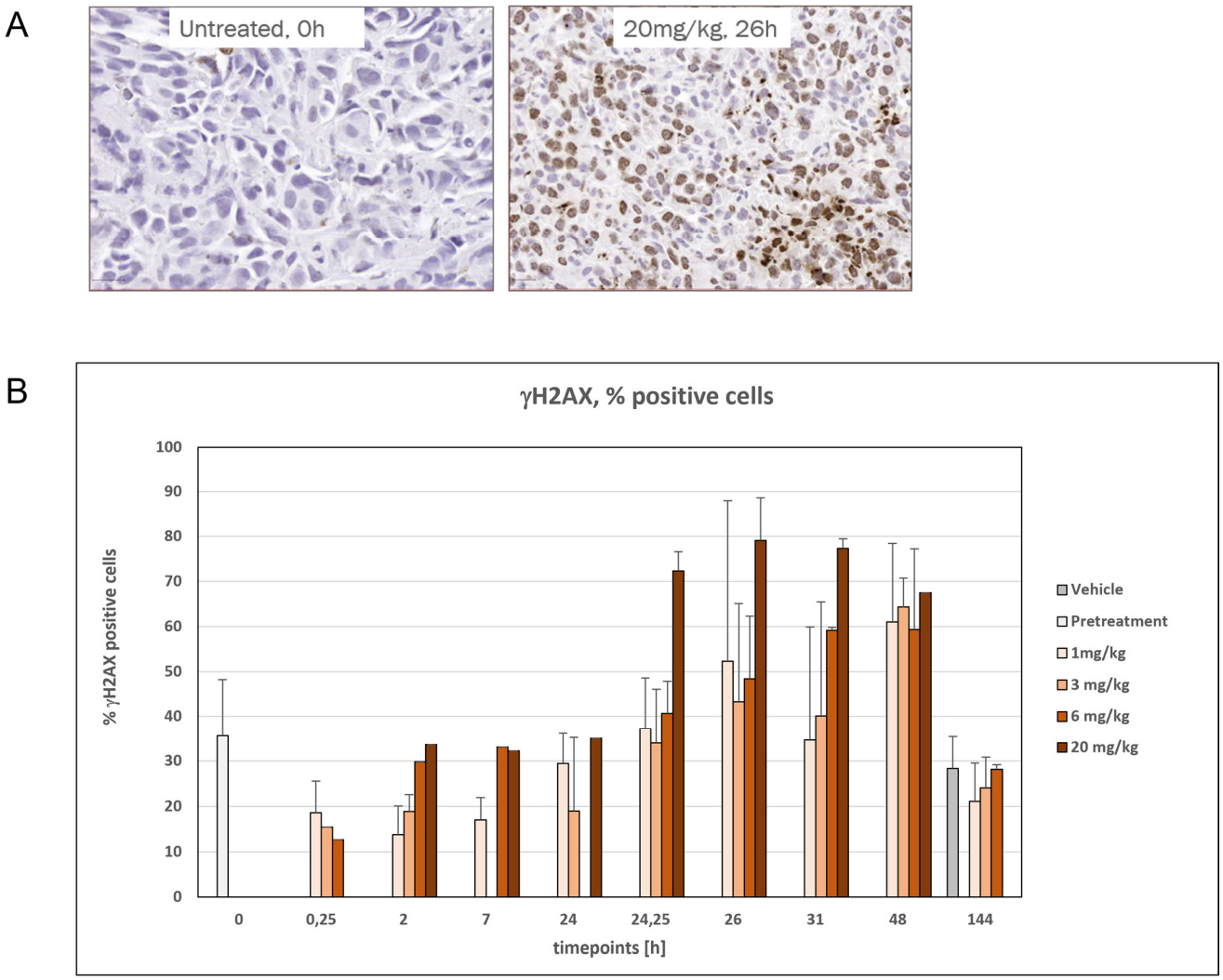

Figure 5. Time- and Dose-Dependent Induction of DNA Damage after Day 1 and Day 2 Dose of VIP236. (**A**) Representative images of gH2AX IHC in tumors from untreated (0 h) and 20 mg/kg treated animals at 26 h post day 1 0 h dose. (**B**) QuPath quantification to score percent positive gH2AX cells by IHC of all tumor samples from animals untreated or treated with vehicle, 1, 3, 6, and 20 mg/kg (dosing occurred on day 1 after 0 h timepoint and on day 2 after 24 h timepoint; 0 h and 24 h timepoint are pretreatment on day 1 and day 2, respectively).

3.7. Monotherapy of VIP236 Achieved Potent and Durable Antitumor Activity in PDX Tumor Mouse Models

VIP236 as monotherapy was investigated in the taxane-resistant PDX lung tumor model LXFL 529 (NSCLC), the clear-cell renal carcinoma tumor model RXF 2667, the liver metastasis of colon tumor model CXF2068, and the TNBC model MAXF BR120, all implanted subcutaneously in NMRI nude mice.

The LXFL 529 model was derived from the primary tumor of a 34-year-old woman with unknown treatment history. In this model, tumor volumes in all therapeutic groups were significantly reduced compared with the control group on day 35 (p-values < 0.0001) (Figure 6A). Tumor volumes in the re-growth phase demonstrated a long-lasting effect of antitumor efficacy. In this model, 40 mg/kg 3 days on and 4 days off was the most

efficacious regimen based on an 100% overall response rate (80% complete response + 20% partial response) (Figure 6E).

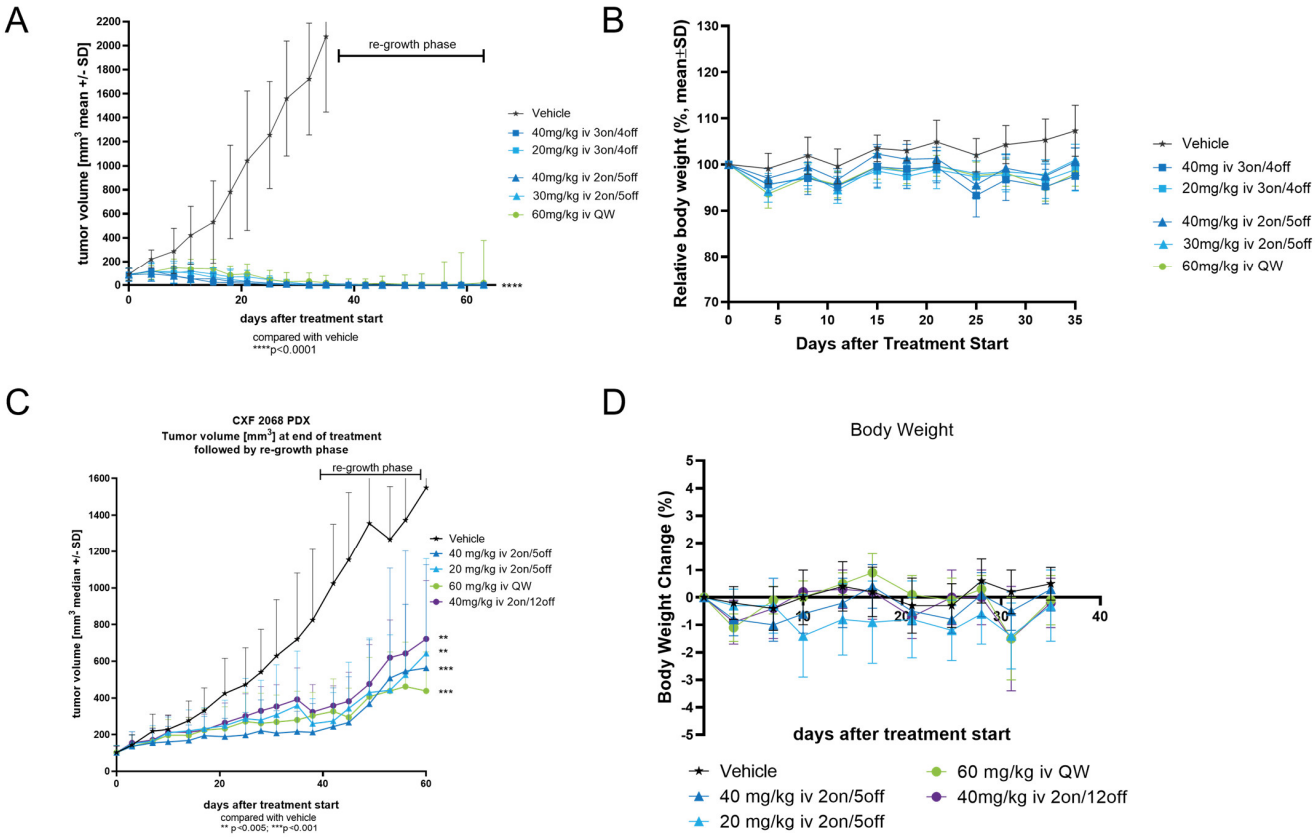

E

Dosing	CR	PR	SD	PD
Vehicle	-	-	-	7
40 mg/kg 3on/4off	8	2	-	-
20 mg/kg 3on/4off	5	5	-	-
40 mg/kg 2on/5off	3	7	-	-
30 mg/kg 2on/5off	6	4	-	-
60 mg/kg QW	2	7	1	-

Figure 6. Tumor growth inhibition with VIP236 monotherapy in PDX mouse models across indications. (**A**) Growth curves of patient-derived lung cancer LXFL529 model. (**B**) Corresponding body weight changes indicate good tolerability of all doses. (**C**) Growth curve of patient-derived liver metastasis of colon cancer CXF 2068 model. Statistically significant tumor growth inhibition ($p < 0.001$ vs. vehicle, $p < 0.005$ vs. vehicle) was observed in this liver metastasis colon PDX model with all schedules. (**D**) Corresponding body weight changes indicate good tolerability of all doses. (**E**) Complete responses in the LXFL529 model were achieved in most treatment groups. All schedules and doses tested exhibit statistical significance; $p < 0.0001$ vs. vehicle. Statistical analysis used unpaired *t*-test. QW, weekly.

The RXF 2667 model was derived from a clear-cell carcinoma of a 61-year-old woman with unknown treatment history. Monotherapy with VIP236 achieved high antitumor efficacy in all treatment groups, including sustained antitumor effect during the regrowth period. (Figure S6A). The CXF 2068 model was derived from liver metastasis from a primary colon cancer tumor of a 50-year-old, previously untreated man. In this model, VIP236 monotherapy at 20/40 mg/kg (2 on/5 off) or at 60 mg/kg (once weekly) reduced tumor volumes significantly in comparison to the control vehicle ($p < 0.001$ Kruskal–Wallis (Figure 6C)). Treatment of VIP236, when administered less frequently at 40 mg/kg

(2 on/12 off), resulted in borderline antitumor efficacy that did not reach statistical significance. The MAXF BR120 was derived from a primary TNBC tumor from a 52-year-old woman after chemotherapy. All VIP236 monotherapy regimens showed statistically significant antitumor efficacy in this model (Figure S6B). VIP236 was well tolerated across PDX models, as evidenced by little weight loss (representative data in Figure 6B,D).

3.8. Significant Impact of VIP236 on Primary Tumor and Metastases in Orthotopic Metastatic TNBC PDX Mouse Models

MA4296 was established from a 43-year-old woman with relapsed squamous metastatic TNBC. MA15191 was derived from a 53-year-old woman with an invasive triple-negative ductal breast carcinoma. Mutation analysis revealed KRAS wild type for both models. The impact of VIP236 monotherapy on tumor growth is shown in Figure 7A,C. Treatment with 40 mg/kg VIP236 (2 on/5 off) resulted in significant tumor growth inhibition of MA4296 (optimum T/C: 4%, day 46, $p < 0.01$; partial remission) and of MA15191 (T/C: 17%, p-value 0.015, Table S3). When given at 60 mg/kg once per week, VIP236 also significantly inhibited orthotopic growth of MA4296 but with reduced efficacy (T/C: 36%, day 36, $p < 0.05$; stable disease) (Table 4). Treatment with both schedules of VIP236 was well tolerated. No early death events occurred, and all mice were in a good general condition, as indicated by the lack of body weight loss (Figure 7B,D).

These PDX models were also chosen to investigate the anti-metastatic effect of VIP236. After termination of the study, mice were inspected for pathologic signs of treatment and for macroscopic metastases at all organs. To look for micrometastasis in lung, brain, and liver tissues, material was prepared from vehicle and treated animals for PCR analyses.

Human DNA was found in lung tissue (moderate expression), brain tissue (low expression), and liver tissue (marginal expression) in both models. In all three organ tissues, treatment with VIP236 reduced the metastatic load compared to the vehicle control. Results of the MA4296 PDX model are depicted in Figure 8. In lung tissue, both doses of VIP236 reduced the ratio of human DNA significantly. Treatment with 40 mg/kg (2 on/5 off) decreased the relative DNA expression highly significantly, with a p-value of <0.0001 and with 60 mg/kg (weekly); thus, a lower but still statistically significant DNA reduction was achieved ($p = 0.032$). In liver tissue samples, a reduction in human DNA load after treatment with 40 mg/kg VIP236 was observed, which did not reach statistical significance. In brain tissue samples, reductions of human DNA were measured, which were statistically significant with 40 mg/kg (2 on/5 off) doses of VIP236 ($p = 0.0067$) but not with 60 mg/kg (weekly). The antimetastatic effect of VIP236 was reproduced in the MA15191 model. These observations may indicate blood–brain barrier penetration of VIP236 and its toxic payload **1**.

3.9. Increase in αvβ3 and NE Staining upon VIP236 Treatment, While TOP1 Expression Is Stable

Due to αvβ3 integrin upregulation during metastasis formation, we specifically investigated the effect of VIP236 treatment in the aforementioned orthotopic TNBC metastasis models [45]. After 4 weeks of treatment with VIP236, the tumors were FFPE-processed to evaluate the presence of αvβ3, NE, and the impact on TOP1 expression. All samples were evaluated by IHC analysis in a semi-quantitative way. The results are summarized in Figure S7. The IHC analysis revealed a rise of αvβ3 presence in the neoplastic cells derived from the orthotopic, metastatic breast cancer PDX model by a higher IHC scoring at treatment end (0.5 to 2.2). Increased infiltration of murine NE occurred from 0.2 to 1.5, while TOP1 expression was stable (3 to 3). These results suggest a positive-feedback loop may occur, producing the durable antitumor efficacy observed in in vivo tumor models.

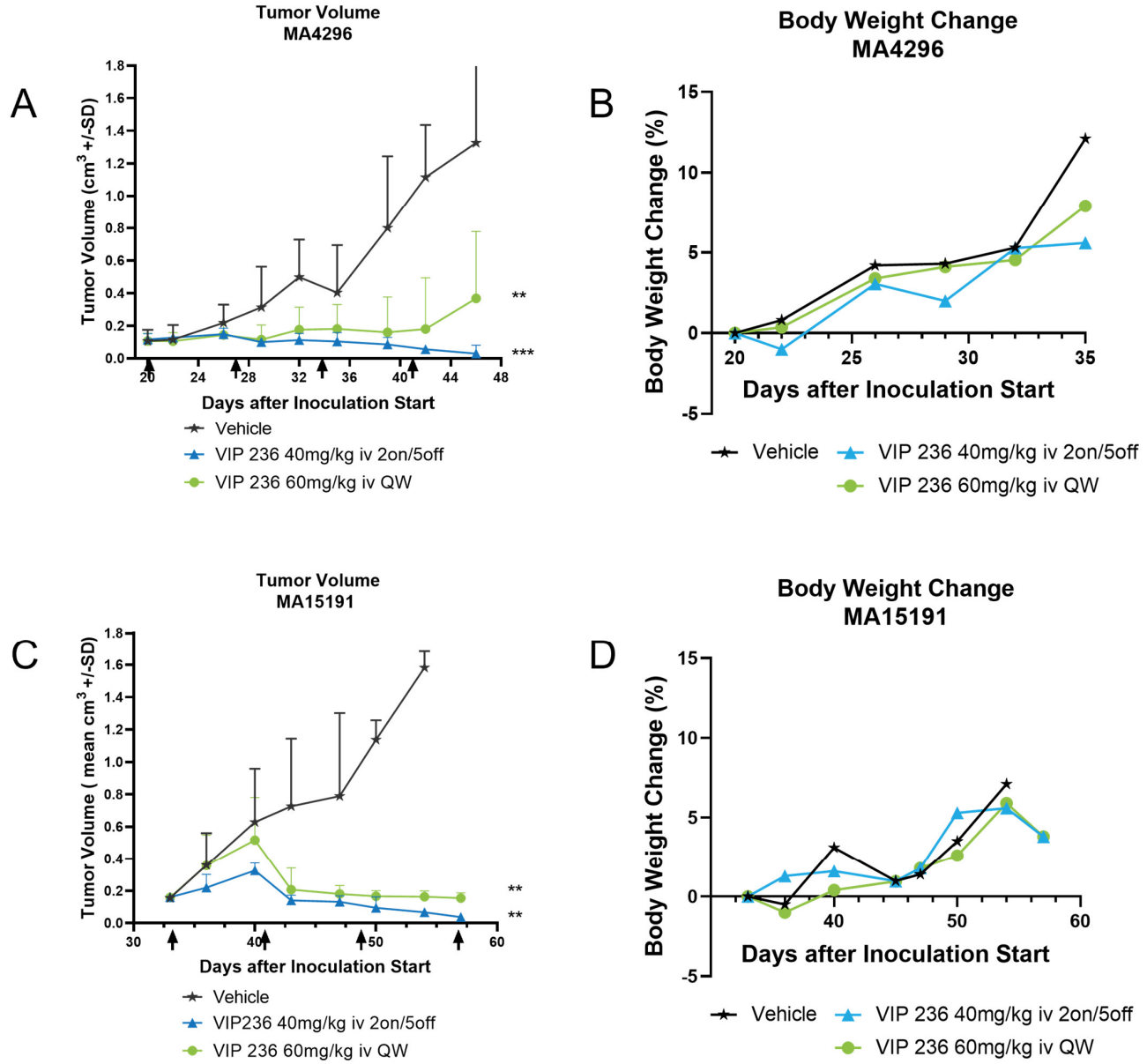

Figure 7. Orthotopic tumor growth of MA4296 (**A**,**B**) and MA15191 (**C**,**D**) in NOG mice and response to VIP236 therapy and bodyweight changes during treatment. Treatment started at 20 days after cell inoculation (day 33). VIP236 was given intravenously at 40 mg/kg (days 1 and 2 × 4 weeks) and at 60 mg/kg once weekly for 4 weeks. Statistical significance: unpaired *t*-test ** $p < 0.01$; *** $p < 0.001$ vs. vehicle. QW, weekly.

Table 4. Summary of treatment data of MA4296 model.

Group	n	Treatment	Route	Treatment Days	Dose (mg/kg)	Opt. T/C (%) (day 46)
A	9	PBS	i.v.	d20, 21, 27, 28, 34, 35, 41, 42		-
B	9	**8** (VIP-236)	i.v.	d20, 21, 27, 28, 34, 35, 41, 42	40	4 **
C	9	**8** (VIP-236)	i.v.	d20, 27, 34, 41	60	36 **

** significant to control (mixed-effects analysis and Tukey's multiple comparisons test).

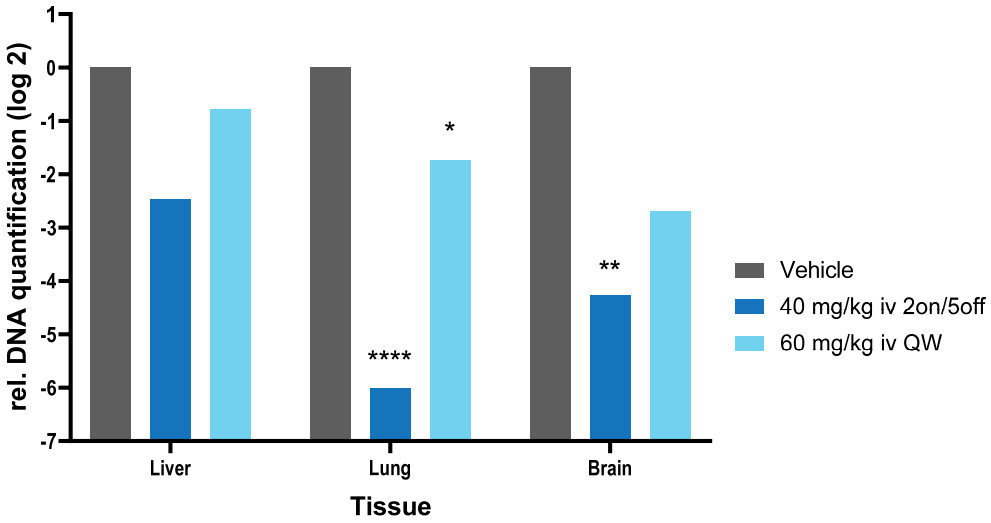

Figure 8. Metastasis formation in MA4296 PDX model. The graphs present relative human DNA expression in lung, liver, and brain samples (n = 10 each) after the indicated treatment. Unpaired *t*-test: **** $p < 0.0001$; ** $p < 0.01$; * $p < 0.05$. QW, weekly.

4. Discussion

VIP236 was designed for targeted delivery of payload **1** to tumors expressing αvβ3 integrins mainly on activated endothelial cells in the TME and for extracellular NE cleavage of the linker to release payload **1**. This design of VIP236 addresses the information gleaned from previous compounds targeting αvβ3 integrins to inhibit angiogenesis, which despite compelling preclinical results, showed only limited efficacy in the clinic, notwithstanding a good safety profile [46–48]. Imaging studies and tissue analysis suggested that αvβ3 integrin inhibitors such as cilengitide and volociximab were highly effective at reaching their intended targets [46]. Therefore, our goal was to leverage the efficient homing of αvβ3 binders and use it for the targeted delivery of a cytotoxic agent to the TME. Our approach does not depend on the inhibition of integrin signaling for its therapeutic effect.

We were able to confirm the tumor homing of the peptidomimetic integrin binder employed in the SMDC VIP236 [34] as well as the tumor localization of NE activity in imaging studies in tumor-bearing mice, which consequently supports the design rational. Furthermore, the high expression of both markers in the TME and their association with aggressive disease and poor prognosis for patients suggests the potential of VIP236 as a pan-solid tumor agent in advanced and metastatic cancers. This potential for broad therapeutic applicability is supported by the activity of VIP236 in PDX tumor models across multiple indications, as previously shown in cell-line-derived models derived from breast, colon, renal, and lung cancers [34]. Here, we demonstrated the high potency of VIP236 monotherapy in a broad panel of PDX models, as exemplified by a long-lasting, complete response in the taxane-resistant NSCLC model LXFL529. Due to upregulation of αvβ3 during metastasis formation, we also specifically investigated the effect of VIP236 in the orthotopic TNBC PDX models MA4296 and MA15191. In addition to a regression of the primary tumor, a significant reduction of micrometastasis in lung and brain tissue was observed.

Other αvβ3-targeted drug conjugates described in the literature [12–16] are designed for activation and drug release mediated by cathepsin or by legumain either intracellularly upon internalization or extracellularly under suboptimal pH conditions. Furthermore, self-immolative spacer groups are often required to enable payload release but associated with an increased lipophilicity of the conjugates. We considered an extracellular release of the payload **1** in the TME as an appropriate match to the αvβ3-mediated delivery and envisioned NE as an appropriate cleavage enzyme to further enhance the targeting specificity of VIP236. Based on publicly available data on NE cleavable probes [49] and leveraging

our previous experience with camptothecin conjugates [50,51], the SMDC VIP236 was optimized for high aqueous solubility, high stability, and efficient cleavability by NE without a need for insertion of self-immolative spacers. Linker length, the carboxy side chain of aspartic acid, and the sterical hindrance of the valine residue with a stabilizing impact on the ester bond contribute to this favorable profile [50]. Irinotecan is a water-soluble prodrug of the TOP1 inhibitor, SN38, which is activated by carboxylesterase to form its active metabolite with higher cleavage efficiency in rodents as compared with humans [39]. In contrast, no decrease in the efficiency of NE-mediated release of the payload is anticipated with VIP236 based on kinetic studies showing similar affinity (Km) of mouse and human NE. In vitro cytotoxicity of VIP236 was found to be NE-dependent. The stability profile was also reflected in pharmacokinetic studies in tumor-bearing mice, with very low levels of released payload detectable in circulation. The SMDC VIP236 has a shorter half-life in comparison to full-sized antibodies and ADCs, but it still shows low clearance and related high exposure and a small volume of distribution. It still delivers payload **1** efficiently to the tumor with a tumor-to-plasma ratio 11-fold higher after administration of VIP236 as compared with administration of an equimolar dose of payload **1** in 786-O tumor-bearing mice. As shown in a study with bile-duct-cannulated rats, almost the entire dose is recovered as unchanged VIP236 in bile. Thus, the main route of elimination of VIP236 in rats appears to be biliary excretion of unchanged VIP236, which is differentiated from the renal excretion of other peptide–drug conjugates [20]. Fourteen ADCs have received marketing approval, most in the last few years, ushering in a new age in "biologic missiles" for targeted cancer therapy [52]. Nonetheless, the application of ADCs for the treatment of solid tumors faces challenges. For example, the large size of ADCs (~ 150 kDa) can hinder deep penetration into the tumor matrix [53]. This inefficient tumor penetration might be the reason why relatively high levels of ADCs are required to achieve efficacy, and consequently, ADCs have not been found to be less toxic than their cytotoxic counterparts [8,54]. Another limitation is that current ADCs require the cell surface expression of a tumor-specific antigen that must also internalize to release the payload. These factors have currently limited the approval of ADCs to a small number of solid tumors that express Her2, Trop2, nectin4, tissue factor, and folate receptor α [55]. Unlike ADCs, VIP236 is a small molecule of ~1.5 kDa and has shown efficient penetration in tumors and affords more than a 10-fold increase in intratumor/plasma payload exposure ratio compared to direct administration of the payload alone. Also, because VIP236 targets αvβ3 and is cleaved extracellularly by NE in TME, it is expected to have broad activity across many tumor types, especially advanced aggressive tumors with the highest unmet medical need. Taken together, these findings support further investigation of VIP236 in clinical trials as a potential treatment option for patients with advanced or invasive solid tumor cancers.

5. Conclusions

VIP236 was designed and optimized for targeting αvβ3 integrins highly expressed on activated endothelial cells in the TME and solid tumors and for extracellular cleavage of an optimized 7-ethyl camptothecin payload **1** by NE. VIP236 shows remarkable chemical, plasma, and metabolic stability. It is selectively cleaved by murine and human NE with similar affinity to release the payload. An 11-fold higher tumor-to-plasma ratio of payload **1** when delivered via VIP236 versus direct IV administration of equimolar amounts of **1** was observed in rats. In contrast, non-cleavable and weakly binding epimers **8e1** and **8e2**, respectively, were not able to accumulate payload **1** in the tumor. Treatment with VIP236 provided durable tumor regressions in NSCLC and CRC PDX models as well as in orthotopic metastatic TNBC PDX models. Importantly, a significant reduction of micrometastasis was observed in lung and brain tissue, providing a platform of evidence for the utility of VIP236 in metastatic disease. VIP236 is currently being evaluated in a first-in-human study in patients with advanced or metastatic solid tumors (NCT05712889).

Supplementary Materials: The following supporting information can be downloaded at: https://www.mdpi.com/article/10.3390/cancers15174381/s1, Figure S1: Stability of VIP236 in PBS; Figure S2: Stability of VIP236 in rat plasma; Figure S3: Michaelis-Menten kinetics of VIP236 in human NE; Figure S4: Michaelis-Menten kinetics of VIP236 in mouse NE; Figure S5: Cytotoxicity of VIP236 and 8e1 and 8e2 in NCI0H292 cell line; Figure S6: Tumor growth curves for RXF 2667 and MAXF BR120 PDX models; Figure S7: Expression of αvβ3 and TOP1; Table S1: Enantiomeric purity of 7 and 7e2; Table S2: PK of VIP236, 8e2 and 8e1 in tumor bearing mice; Table S3: Summary of treatment and T/C on MA15191 PDX model.

Author Contributions: Conceptualization, H.-G.L., B.S.-L., M.H. and D.Z.; methodology, M.H., B.S.-L., D.Z., H.-G.L., K.M.G. and M.M.F.; investigation, B.S.-L., M.H., D.Z., H.-G.L., K.M.G. and M.M.F.; writing—original draft preparation, H.-G.L., B.S.-L., H.W., M.M.F., D.Z. and K.M.G.; writing—review and editing, R.I., H.W., H.-G.L., B.S.-L., M.M.F., D.Z., K.M.G. and A.J.J.; supervision, H.-G.L. and A.H.; project administration, H.-G.L. and B.S.-L.; funding acquisition, A.H. All authors have read and agreed to the published version of the manuscript.

Funding: This research received no external funding.

Institutional Review Board Statement: In accordance with the standard practice for drug discovery studies where compliance with good laboratory practice (GLP) is not required, these studies were conducted as a non-GLP study. The studies were conducted according to all applicable international, national, and local laws and followed the national guidelines for the Care and Use of Laboratory Animals of the Society of Laboratory Animal Science (GV-SOLAS). All animal experiment protocols were approved by the regional council Committee on the Ethics of Animal Experiments (Protocol code: G20/163, 11 May 2021, 24 August 2021, 27 May 2022 and 7 February 2023).

Informed Consent Statement: Not applicable.

Data Availability Statement: The data can be shared upon request.

Acknowledgments: This paper is dedicated to the memory of Jörg Keldenich, and we thank him for his role in planning and pursuing DMPK studies. We thank Bendix, S., Boldt, T., DiBetta, A.-M., Koenig, B., Lindner, H., Swifka, J. and Wolter, D. for excellent technical assistance and Koebberling, J. for the supervision. We thank Nuvisan, ICB, CRL, provitro, and epo-berlin and in particular Erkelenz, M., Siemeister, G., Litzenburger, U., Reuvers, M., and Behrens, D. for performing in vitro and in vivo studies. Special thanks to Zhang, X., Soltani, O., Lerchen, A., Becker, C. and Zeller, J. for supporting the upscale of the VIP236 synthesis as well as Tsithenge, D., Spang, R.,Voits, P., Schneider, D., and Stoltefuss, M. for thoughtful analytical support.

Conflicts of Interest: Hans-Georg Lerchen, Beatrix Stelte-Ludwig, Melanie M. Frigault, Amy J. Johnson, Raquel Izumi, and Ahmed Hamdy are employees of and own stock in Vincerx Pharma. Harvey Wong is a consultant for Vincerx Pharma. Hans-Georg Lerchen, Melanie Heroult, Dmitry Zubov, and Kersten Matthias Gericke own stock in Bayer AG.

References

1. Schwartz, R.S. Paul Ehrlich's Magic Bullets. *N. Engl. J. Med.* **2004**, *350*, 1079–1080. [CrossRef]
2. Dean, A.Q.; Luo, S.; Twomey, J.D.; Zhang, B. Targeting Cancer with Antibody-Drug Conjugates: Promises and Challenges. *mAbs* **2021**, *13*, 1951427. [CrossRef] [PubMed]
3. Baah, S.; Laws, M.; Rahman, K.M. Antibody–Drug Conjugates—A Tutorial Review. *Molecules* **2021**, *26*, 2943. [CrossRef] [PubMed]
4. Drago, J.Z.; Modi, S.; Chandarlapaty, S. Unlocking the Potential of Antibody–Drug Conjugates for Cancer Therapy. *Nat. Rev. Clin. Oncol.* **2021**, *18*, 327–344. [CrossRef]
5. Conilh, L.; Sadilkova, L.; Viricel, W.; Dumontet, C. Payload Diversification: A Key Step in the Development of Antibody–Drug Conjugates. *J. Hematol. Oncol.* **2023**, *16*, 3. [CrossRef]
6. Modi, S.; Jacot, W.; Yamashita, T.; Sohn, J.; Vidal, M.; Tokunaga, E.; Tsurutani, J.; Ueno, N.T.; Prat, A.; Chae, Y.S.; et al. Trastuzumab Deruxtecan in Previously Treated HER2-Low Advanced Breast Cancer. *N. Engl. J. Med.* **2022**, *387*, 9–20. [CrossRef]
7. Rugo, H.S.; Bardia, A.; Tolaney, S.M.; Arteaga, C.; Cortes, J.; Sohn, J.; Marmé, F.; Hong, Q.; Delaney, R.J.; Hafeez, A.; et al. TROPiCS-02: A Phase III Study Investigating Sacituzumab Govitecan in the Treatment of HR+/HER2− Metastatic Breast Cancer. *Future Oncol.* **2020**, *16*, 705–715. [CrossRef] [PubMed]
8. Colombo, R.; Rich, J.R. The Therapeutic Window of Antibody Drug Conjugates: A Dogma in Need of Revision. *Cancer Cell* **2022**, *40*, 1255–1263. [CrossRef]
9. Zhuang, C.; Guan, X.; Ma, H.; Cong, H.; Zhang, W.; Miao, Z. Small Molecule-Drug Conjugates: A Novel Strategy for Cancer-Targeted Treatment. *Eur. J. Med. Chem.* **2019**, *163*, 883–895. [CrossRef]

10. Cazzamalli, S.; Dal Corso, A.; Widmayer, F.; Neri, D. Chemically-Defined Antibody- and Small Molecule-Drug Conjugates for in Vivo Tumor Targeting Applications: A Comparative Analysis. *J. Am. Chem. Soc.* **2018**, *140*, 1617–1621. [CrossRef]
11. Reddy, J.A.; Dorton, R.; Westrick, E.; Dawson, A.; Smith, T.; Xu, L.-C.; Vetzel, M.; Kleindl, P.; Vlahov, I.R.; Leamon, C.P. Preclinical Evaluation of EC145, a Folate-Vinca Alkaloid Conjugate. *Cancer Res.* **2007**, *67*, 4434–4442. [CrossRef] [PubMed]
12. Liu, Y.; Bajjuri, K.M.; Liu, C.; Sinha, S.C. Targeting Cell Surface Alpha(v)Beta(3) Integrins Increases Therapeutic Efficacies of a Legumain Protease-Activated Auristatin Prodrug. *Mol. Pharm.* **2012**, *9*, 168–175. [CrossRef] [PubMed]
13. Alloatti, D.; Giannini, G.; Vesci, L.; Castorina, M.; Pisano, C.; Badaloni, E.; Cabri, W. Camptothecins in Tumor Homing via an RGD Sequence Mimetic. *Bioorg. Med. Chem. Lett.* **2012**, *22*, 6509–6512. [CrossRef] [PubMed]
14. Raposo Moreira Dias, A.; Pina, A.; Dean, A.; Lerchen, H.; Caruso, M.; Gasparri, F.; Fraietta, I.; Troiani, S.; Arosio, D.; Belvisi, L.; et al. Neutrophil Elastase Promotes Linker Cleavage and Paclitaxel Release from an Integrin-Targeted Conjugate. *Chem. Weinh. Bergstr. Ger.* **2019**, *25*, 1696–1700. [CrossRef]
15. Paulus, J.; Sewald, N. Synthesis and Evaluation of a Non-Peptide Small-Molecule Drug Conjugate Targeting Integrin αVβ3. *Front. Chem.* **2022**, *10*, 869639. [CrossRef]
16. Paulus, J.; Nachtigall, B.; Meyer, P.; Sewald, N. RGD Peptidomimetic MMAE-Conjugate Addressing Integrin αVβ3-Expressing Cells with High Targeting Index. *Chem. Eur. J.* **2023**, *29*, e202203476. [CrossRef]
17. Cazzamalli, S.; Figueras, E.; Pethő, L.; Borbély, A.; Steinkühler, C.; Neri, D.; Sewald, N. In Vivo Antitumor Activity of a Novel Acetazolamide–Cryptophycin Conjugate for the Treatment of Renal Cell Carcinomas. *ACS Omega* **2018**, *3*, 14726–14731. [CrossRef]
18. Whalen, K.A.; White, B.H.; Quinn, J.M.; Kriksciukaite, K.; Alargova, R.; Au Yeung, T.P.; Bazinet, P.; Brockman, A.; DuPont, M.M.; Oller, H.; et al. Targeting the Somatostatin Receptor 2 with the Miniaturized Drug Conjugate, PEN-221: A Potent and Novel Therapeutic for the Treatment of Small Cell Lung Cancer. *Mol. Cancer Ther.* **2019**, *18*, 1926–1936. [CrossRef]
19. Millul, J.; Bassi, G.; Mock, J.; Elsayed, A.; Pellegrino, C.; Zana, A.; Dakhel Plaza, S.; Nadal, L.; Gloger, A.; Schmidt, E.; et al. An Ultra-High-Affinity Small Organic Ligand of Fibroblast Activation Protein for Tumor-Targeting Applications. *Proc. Natl. Acad. Sci. USA* **2021**, *118*, e2101852118. [CrossRef]
20. Bennett, G.; Brown, A.; Mudd, G.; Huxley, P.; van Rietschoten, K.; Pavan, S.; Chen, L.; Watcham, S.; Lahdenranta, J.; Keen, N. MMAE Delivery Using the Bicycle Toxin Conjugate BT5528. *Mol. Cancer Ther.* **2020**, *19*, 1385–1394. [CrossRef]
21. Currie, J.-C.; Demeule, M.; Charfi, C.; Zgheib, A.; Larocque, A.; Danalache, B.A.; Ouanouki, A.; Béliveau, R.; Marsolais, C.; Annabi, B. The Peptide-Drug Conjugate TH1902: A New Sortilin Receptor-Mediated Cancer Therapeutic against Ovarian and Endometrial Cancers. *Cancers* **2022**, *14*, 1877. [CrossRef]
22. Mudd, G.E.; Scott, H.; Chen, L.; van Rietschoten, K.; Ivanova-Berndt, G.; Dzionek, K.; Brown, A.; Watcham, S.; White, L.; Park, P.U.; et al. Discovery of BT8009: A Nectin-4 Targeting Bicycle Toxin Conjugate for the Treatment of Cancer. *J. Med. Chem.* **2022**, *65*, 14337–14347. [CrossRef] [PubMed]
23. Cooper, J.; Giancotti, F.G. Integrin Signaling in Cancer: Mechanotransduction, Stemness, Epithelial Plasticity, and Therapeutic Resistance. *Cancer Cell* **2019**, *35*, 347–367. [CrossRef] [PubMed]
24. Desgrosellier, J.S.; Cheresh, D.A. Integrins in Cancer: Biological Implications and Therapeutic Opportunities. *Nat. Rev. Cancer* **2010**, *10*, 9–22. [CrossRef] [PubMed]
25. Danhier, F.; Le Breton, A.; Préat, V. RGD-Based Strategies To Target Alpha(v) Beta(3) Integrin in Cancer Therapy and Diagnosis. *Mol. Pharm.* **2012**, *9*, 2961–2973. [CrossRef]
26. Hieken, T.J.; Farolan, M.; Ronan, S.G.; Shilkaitis, A.; Wild, L.; Gupta, T.K.D. β3 Integrin Expression in Melanoma Predicts Subsequent Metastasis. *J. Surg. Res.* **1996**, *63*, 169–173. [CrossRef]
27. Sun, F.; Wang, J.; Sun, Q.; Li, F.; Gao, H.; Xu, L.; Zhang, J.; Sun, X.; Tian, Y.; Zhao, Q.; et al. Interleukin-8 Promotes Integrin B3 Upregulation and Cell Invasion through PI3K/Akt Pathway in Hepatocellular Carcinoma. *J. Exp. Clin. Cancer Res.* **2019**, *38*, 449. [CrossRef]
28. Wu, C.-M.; Li, T.-M.; Tan, T.-W.; Fong, Y.-C.; Tang, C.-H. Berberine Reduces the Metastasis of Chondrosarcoma by Modulating the $\alpha v\beta 3$ Integrin and the PKCδ, c-Src, and AP-1 Signaling Pathways. *Evid. Based Complement. Alternat. Med.* **2013**, *2013*, e423164. [CrossRef]
29. Korkmaz, B.; Moreau, T.; Gauthier, F. Neutrophil Elastase, Proteinase 3 and Cathepsin G: Physicochemical Properties, Activity and Physiopathological Functions. *Biochimie* **2008**, *90*, 227–242. [CrossRef]
30. Uhlén, M.; Fagerberg, L.; Hallström, B.M.; Lindskog, C.; Oksvold, P.; Mardinoglu, A.; Sivertsson, Å.; Kampf, C.; Sjöstedt, E.; Asplund, A.; et al. Tissue-Based Map of the Human Proteome. *Science* **2015**, *347*, 1260419. [CrossRef]
31. Sato, T.; Takahashi, S.; Mizumoto, T.; Harao, M.; Akizuki, M.; Takasugi, M.; Fukutomi, T.; Yamashita, J. Neutrophil Elastase and Cancer. *Surg. Oncol.* **2006**, *15*, 217–222. [CrossRef] [PubMed]
32. Mohamed Amar, I.A.; Huvelle, S.; Douez, E.; Letast, S.; Henrion, S.; Viaud-Massuard, M.-C.; Aubrey, N.; Allard-Vannier, E.; Joubert, N.; Denevault-Sabourin, C. Dual Intra- and Extracellular Release of Monomethyl Auristatin E from a Neutrophil Elastase-Sensitive Antibody-Drug Conjugate. *Eur. J. Med. Chem.* **2022**, *229*, 114063. [CrossRef]
33. Dornan, D.; Kudirka, R.; Safina, B.; Zhou, M. Elastase-Substrate, Peptide Linker Immunoconjugates, and Uses Thereof. WO2021226440A1, 7 May 2021.
34. Lerchen, H.-G.; Stelte-Ludwig, B.; Kopitz, C.; Heroult, M.; Zubov, D.; Willuda, J.; Schlange, T.; Kahnert, A.; Wong, H.; Izumi, R.; et al. A Small Molecule–Drug Conjugate (SMDC) Consisting of a Modified Camptothecin Payload Linked to an αVß3 Binder for the Treatment of Multiple Cancer Types. *Cancers* **2022**, *14*, 391. [CrossRef] [PubMed]

35. Perrier, D.; Gibaldi, M. General Derivation of the Equation for Time to Reach a Certain Fraction of Steady State. *J. Pharm. Sci.* **1982**, *71*, 474–475. [CrossRef] [PubMed]
36. Becker, M.; Nitsche, A.; Neumann, C.; Aumann, J.; Junghahn, I.; Fichtner, I. Sensitive PCR Method for the Detection and Real-Time Quantification of Human Cells in Xenotransplantation Systems. *Br. J. Cancer* **2002**, *87*, 1328–1335. [CrossRef]
37. Sawada, S.; Matsuoka, S.; Nokata, K.; Nagata, H.; Furuta, T.; Yokokura, T.; Miyasaka, T. Synthesis and Antiumor Activity of 20(S)-Camptothecin Derivatives: A-Ring Modified and 7, 10-Disubstituted Camptothecins. *Chem. Pharm. Bull.* **1991**, *39*, 3183–3188. [CrossRef]
38. Kunimoto, T.; Nitta, K.; Tanaka, T.; Uehara, N.; Baba, H.; Takeuchi, M.; Yokokura, T.; Sawada, S.; Miyasaka, T.; Mutai, M. Antitumor Activity of 7-Ethyl-10-[4-(1-Piperidino)-1-Piperidino]Carbonyloxycamptothecin, a Novel Water-Soluble Derivative of Camptothecin, against Murine Tumors1. *Cancer Res.* **1987**, *47*, 5944–5947.
39. Ramesh, M.; Ahlawat, P.; Srinivas, N.R. Irinotecan and Its Active Metabolite, SN-38: Review of Bioanalytical Methods and Recent Update from Clinical Pharmacology Perspectives. *Biomed. Chromatogr.* **2010**, *24*, 104–123. [CrossRef]
40. Lerchen, H.-G.; Stelte-Ludwig, B.; Kopitz, C.; Keldenich, J. Cytostatic Conjugates with Integrin Ligands. WO/2020/094471, 14 May 2020.
41. Davies, B.; Morris, T. Physiological Parameters in Laboratory Animals and Humans. *Pharm. Res.* **1993**, *10*, 1093–1095. [CrossRef]
42. Vonlaufen, A.; Wiedle, G.; Borisch, B.; Birrer, S.; Luder, P.; Imhof, B.A. Integrin αvβ3 Expression in Colon Carcinoma Correlates with Survival. *Mod. Pathol.* **2001**, *14*, 1126–1132. [CrossRef]
43. Ha, S.Y.; Shin, J.; Kim, J.H.; Kang, M.S.; Yoo, H.-Y.; Kim, H.-H.; Um, S.-H.; Kim, S.-H. Overexpression of Integrin αv Correlates with Poor Prognosis in Colorectal Cancer. *J. Clin. Pathol.* **2014**, *67*, 576–581. [CrossRef] [PubMed]
44. Chatterjee, N.; Walker, G.C. Mechanisms of DNA Damage, Repair, and Mutagenesis. *Environ. Mol. Mutagen.* **2017**, *58*, 235–263. [CrossRef]
45. Desgrosellier, J.S.; Barnes, L.A.; Shields, D.J.; Huang, M.; Lau, S.K.; Prévost, N.; Tarin, D.; Shattil, S.J.; Cheresh, D.A. Integrin αvβ3/c-Src "Oncogenic Unit" Promotes Anchorage-Independence and Tumor Progression. *Nat. Med.* **2009**, *15*, 1163–1169. [CrossRef] [PubMed]
46. Alday-Parejo, B.; Stupp, R.; Rüegg, C. Are Integrins Still Practicable Targets for Anti-Cancer Therapy? *Cancers* **2019**, *11*, 978. [CrossRef] [PubMed]
47. Hatley, R.J.D.; Macdonald, S.J.F.; Slack, R.J.; Le, J.; Ludbrook, S.B.; Lukey, P.T. An αv-RGD Integrin Inhibitor Toolbox: Drug Discovery Insight, Challenges and Opportunities. *Angew. Chem. Int. Ed.* **2018**, *57*, 3298–3321. [CrossRef] [PubMed]
48. Ludwig, B.S.; Kessler, H.; Kossatz, S.; Reuning, U. RGD-Binding Integrins Revisited: How Recently Discovered Functions and Novel Synthetic Ligands (Re-)Shape an Ever-Evolving Field. *Cancers* **2021**, *13*, 1711. [CrossRef]
49. Achilles, K.; Bednarski, P.J. Quantification of Elastase-Like Activity in 13 Human Cancer Cell Lines and in an Immortalized Human Epithelial Cell Line by RP-HPLC. *Biol. Chem.* **2003**, *384*, 817–824. [CrossRef]
50. Lerchen, H.-G.; von dem Bruch, K. Synthesis of 20-O-Linked 20(S)-Camptothecin Glycoconjugates: Impact of the Side Chain of the Ester-Linked Amino Acid on Epimerization During the Acylation Reaction and on Hydrolytic Stability of the Final Glycoconjugates. *J. Prakt. Chem.* **2000**, *342*, 753–760. [CrossRef]
51. Lerchen, H.-G.; Baumgarten, J.; von dem Bruch, K.; Lehmann, T.E.; Sperzel, M.; Kempka, G.; Fiebig, H.-H. Design and Optimization of 20-O-Linked Camptothecin Glycoconjugates as Anticancer Agents. *J. Med. Chem.* **2001**, *44*, 4186–4195. [CrossRef]
52. Fu, Z.; Li, S.; Han, S.; Shi, C.; Zhang, Y. Antibody Drug Conjugate: The "Biological Missile" for Targeted Cancer Therapy. *Signal Transduct. Target. Ther.* **2022**, *7*, 93. [CrossRef]
53. Tsumura, R.; Manabe, S.; Takashima, H.; Koga, Y.; Yasunaga, M.; Matsumura, Y. Influence of the Dissociation Rate Constant on the Intra-Tumor Distribution of Antibody-Drug Conjugate against Tissue Factor. *J. Control. Release* **2018**, *284*, 49–56. [CrossRef] [PubMed]
54. Tarantino, P.; Ricciuti, B.; Pradhan, S.M.; Tolaney, S.M. Optimizing the Safety of Antibody–Drug Conjugates for Patients with Solid Tumours. *Nat. Rev. Clin. Oncol.* **2023**, *20*, 558–576. [CrossRef] [PubMed]
55. Dumontet, C.; Reichert, J.M.; Senter, P.D.; Lambert, J.M.; Beck, A. Antibody–Drug Conjugates Come of Age in Oncology. *Nat. Rev. Drug Discov.* **2023**, *22*, 641–661. [CrossRef] [PubMed]